The Astrophysical Journal, 668:1246–1258, 2007 October 20
© 2007. The American Astronomical Society. All rights reserved. Printed in U.S.A.

MAGNETIC FIELDS IN THE HELIOSHEATH AND DISTANT HELIOSPHERE: *VOYAGER 1* AND *2* OBSERVATIONS DURING 2005 AND 2006

L. F. Burlaga,[1] N. F. Ness,[2] and M. H. Acuña[3]

Received 2007 March 30; accepted 2007 June 27

ABSTRACT

This paper examines the variability of daily averages of the magnetic field strength B in the heliosheath and in the distant solar wind measured by *Voyager 1* (*V1*) and *Voyager 2* (*V2*), respectively, from 2005.0 to 2006.9. In the heliosheath, a spatial gradient of (0.0023 ± 0.0011) nT AU^{-1} is observed, which constrains models of the inner heliosheath. This gradent is small compared to the expected average gradient of B across the entire heliosheath. In the heliosheath the profile of B is generally filamentary with numerous jumps, but a large-amplitude sine wave with a period of $\approx$200 days was observed by *V1* at the end of the interval. The fluctuations of daily averages of B observed by *V1* and *V2* have a Gaussian distribution and lognormal distribution, respectively. The autocorrelation of $B(t)$ from day of year (DOY) 1–512 was an exponential function with an e-folding time of $\approx 3.7 \pm 0.5$ days for *V1* and 2.5 ± 0.3 days for *V2*. On scales from 1–4 days, the autocorrelation function was a power law with exponent $\alpha = -0.440 \pm 0.031$ for *V1* and $\alpha = -0.497 \pm 0.002$ for *V2*. The distribution of differences of successive daily averages of B for both *V1* and *V2* is the Tsallis distribution of nonextensive statistical mechanics with the nonextensivity parameter $q = 1.55 \pm 0.05$. *V2* (at $\approx$S26°) observed both positive and negative magnetic polarities throughout the interval from 2005.0 to 2006.9. There is evidence that *V1* (at N34°) might be entering a region of negative magnetic polarity as the latitudinal extent of the heliospheric current sheet decreases during the declining phase of solar cycle 23.

Subject headings: magnetic fields — MHD — solar wind — turbulence

1. INTRODUCTION

Voyager 1 (*V1*) crossed the termination shock on 2004 December 16 ± 1 the uncertainty being due to a data gap (Stone et al. 2005; Gurnett & Kurth 2005; Decker et al. 2005; Burlaga et al. 2005), and it has been moving in the heliosheath since that time. The heliosheath is a region extending from the termination shock to the interstellar medium (Axford 1972; Parker 1963; Hundhausen 1972; Zank 1999). Models of the termination shock and heliosheath have been presented by Liewer et al. (1993, 1996), Leroy (1983), Whang et al. (1995), Pauls et al. (1995), Müller et al. (2006), Opher et al. (2004, 2006), Izmodenov et al. (2005), Izmodenov & Alexashov (2006), Nerney et al. (1991, 1993, 1995), Pogorelov (2006), Pogorelov et al. (2006), Washimi (1993), Washimi & Tanaka (1996, 1999), Tanaka & Washimi (1999), Zank (1999), and Zank et al. (1996).

A significant feature of the magnetic fields observed in the heliosheath is the large variability of the magnetic field strength B. On very small scales, *V1* observes magnetic holes and humps in which B changes on a scale of the order of 1 hr (Burlaga et al. 2006a). The distributions of hourly and daily magnetic field strengths in the heliosheath were Gaussian in the interval 2005 day of year (DOY) 1–125 (Burlaga et al. 2005, 2006b). Large, non-Gaussian jumps in B as well as smaller Gaussian changes in B are observed, and the distribution of increments of daily averages of B is described by the Tsallis probability function of nonextensive statistical mechanics (Burlaga et al. 2006d). The large jumps are related to a filamentary structure is observed in $B(t)$ on a scale of days (Burlaga et al. 2006c).

This paper analyzes and compares the large-scale structure of the magnetic field $\boldsymbol{B}$ on scales between 1 day and $\approx$700 days in the heliosheath (observed by *V1* from 2005.0 to 2006.90) and in the distant supersonic solar wind (observed by *Voyager 2* [*V2*] from 2005.00 to 2006.92). *V1* moved from radial distance $R =$ 94.17 AU and latitude N34.1° at 2005.0 to $R = 101.36$ AU and latitude N34.2° at 2007.0. *V2* moved from $R = 75.31$ AU and latitude S25.7° at 2005.0 to $R = 81.57$ AU and latitude S27.1° at 2007.0. Magnetic field observations have been made by the magnetic field experiment on *V1* and *V2* (Behannon et al. 1977) from launch in 1977 to present. Owing to gaps in the data coverage by the Deep Space Network, data are available for only $\approx$8–16 hr each day. On some days, such as when *V1* crossed the termination shock, no data are available.

Evidence for a small linear increase in B with increasing distance from the Sun in the heliosheath is presented in § 2. The gradient in B observed for 700 days behind the termination shock (TS) is small compared to the predicted average gradient between the TS and heliopause. Section 3 shows that the fluctuations of B about the linear trend observed by *V1* are Gaussian, but the width of the Gaussian depends on the length of the interval considered. The corresponding fluctuations of B observed by *V2* in the distant heliosphere have lognormal distributions, which are characteristic of the supersonic solar wind.

The autocorrelation function $C(\tau)$ of $B(t)$ measured by *V1* in the heliosheath and by *V2* in the distant supersonic solar wind during the intervals DOY 1–695 and DOY 1–512 is discussed in § 4. The distribution of increments of B observed by *V1* and *V2* is discussed in § 5. Section 6 shows that from 2005.0 to 2006.9 *V2*, at $\approx$S26°, observed a uniform distribution of positive and negative polarity, whereas *V1*, at N34°, observed a trend toward increasing negative polarity. The change of polarity observed by *V1* might be related to the decreasing latitudinal extent of the heliospheric current sheet during the declining phase of the solar cycle.

2. LARGE-SCALE RADIAL VARIATIONS OF THE MAGNETIC FIELD IN THE HELIOSHEATH

Observations of the magnetic field $\boldsymbol{B}$ observed by *V1* in the 695 day interval from 2005 DOY 1 (2005.0) to 2006 DOY 330

[1] NASA/Goddard Space Flight Center, Geospace Physics Laboratory, Code 673, Greenbelt, MD 20771; leonard.f.burlaga@nasa.gov.
[2] Institute for Astrophysics and Computational Sciences, Catholic University of America, Washington, DC 20064; nfnudel@yahoo.com.
[3] NASA/Goddard Space Flight Center, Planetary Magnetospheres Laboratory, Code 695, Greenbelt, MD 20771; mario.h.acuna@nasa.gov.

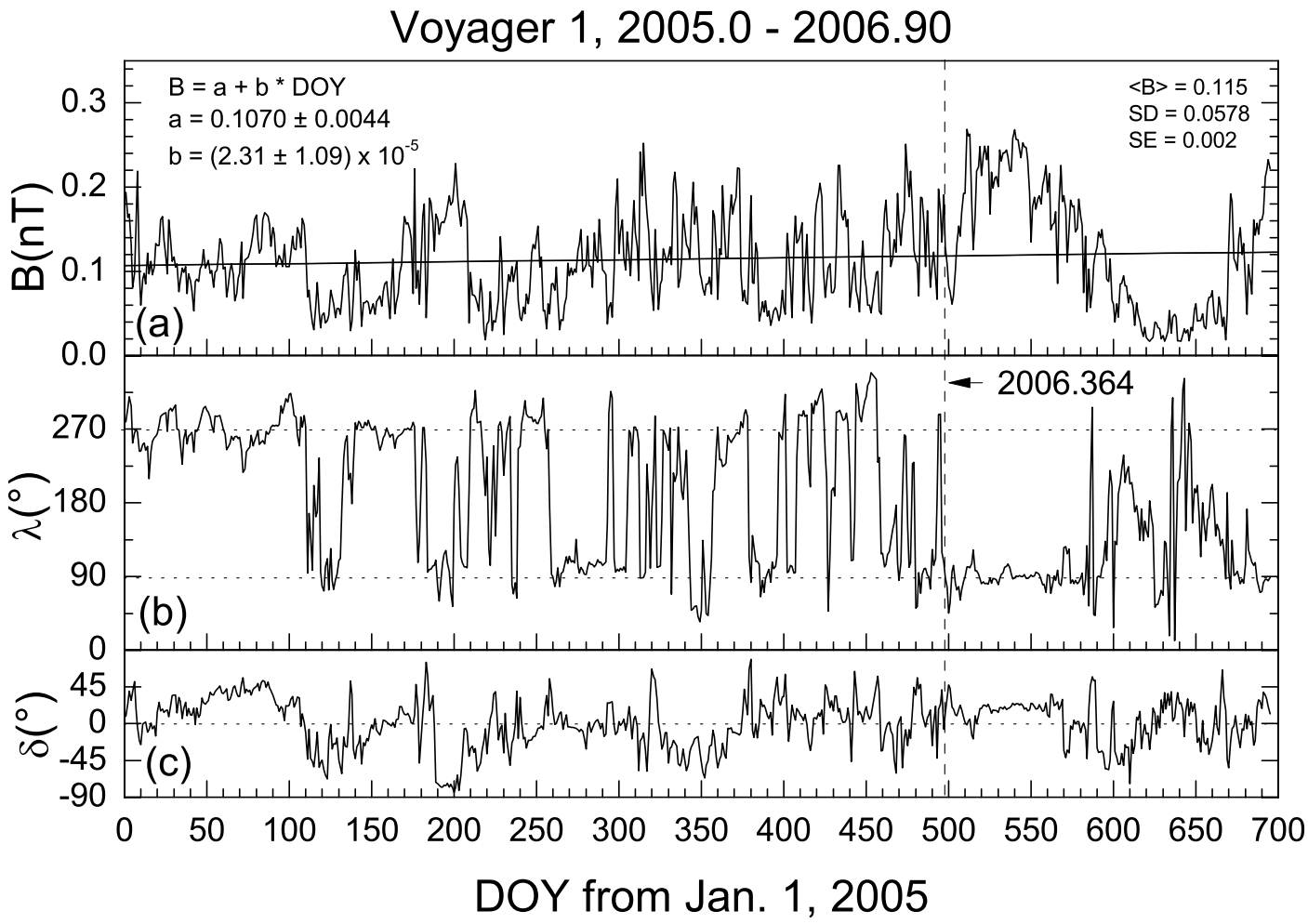


FIG. 1.—*V1* observations of daily averages of (*a*) the magnetic field strength *B* in nanoteslas, (*b*) azimuthal angle λ, and (*c*) elevation angles δ.

(2006.90) are shown in Figure 1. It is convenient to discuss intervals in terms of integer units of days; we shall write "DOY A–B" as an abbreviation for the interval from DOY A to DOY B measured relative to 2005 January 1 = DOY 1. Data are missing for only 7 of the days in this interval, but there are typically gaps of ≈8–16 hr on each day owing to limitations on tracking of the spacecraft. The daily averages of *B*, azimuthal angle λ, and elevation angle δ are shown in Figures 1*a*, 1*b*, and 1*c*, respectively. The angles are in heliographic (HG) coordinates (see, e.g., Figs. 1 and 2 in Burlaga 1995). The observations in Figure 1 represent the "fully processed" data containing all of the calibrations and corrections that are required to derive the highest quality data that were available at the time this paper was written. The representative error bars on *B* are ≈±0.015 nT, the estimated 1 σ error due to both systematic and random effects. For individual measurements the uncertainties can be smaller or larger, but it is not possible in general to estimate these uncertainties more accurately. The average magnetic field strength in this 695 day interval is $\langle B \rangle = 0.115 \pm 0.002$ nT, where the uncertainty here is the standard error in the mean. The standard deviation is SD = 0.058 nT, and the minimum and maximum values of *B* are 0.018 and 0.269 nT, respectively.

As described by Burlaga et al. (2005, 2006b, 2006d) there are large fluctuations in the $B(t)$ in the heliosheath, and there appears to be a filamentary structure. Most notable is the new feature in $B(t)$ from ≈DOY 500 to 695; this variation is approximately one cycle of a sine wave, $A \sin [2\pi(t - t_o)/\tau]$, with amplitude $A \approx 0.12$ nT, period $\tau \approx 200$ days, and $t_o \approx 490$ days. Inspection of Figure 1*a* suggests that there might also be a larger scale feature, a tendency for the *B* to increase across the entire 695 day interval. This is confirmed by a linear least-squares fit, which gives the straight line shown in Figure 1*a*. The slope of this line is $s_{V1} = (2.31 \pm 1.09) \times 10^{-5}$ nT day^{-1} = (0.0084 ± 0.0040) nT yr^{-1}, which is significant at the 1 σ level, but not at the 2 σ level.

It might be argued that the increasing *B* indicated by the fit in Figure 1*a* is simply a temporal variation, such as a solar cycle variation. If this were the case, then one would expect to observe a similar increase at 1 AU. Figure 2 shows $B(t)$ measured at 1 AU by the *Advanced Composition Explorer* (*ACE*) spacecraft from 2004.0 to 2006.5. The transit time of the solar wind from 1 AU to the position of *V1* is approximately 1 yr. The straight line in Figure 2 shows a linear fit of the *ACE* observations from 2004.0 to 2006.0. The slope of this line is $s_{ACE} = (-0.44 \pm 0.20)$ nT yr^{-1}. Thus, *B* is decreasing with increasing time at 1 AU, as one expects during the declining phase of the solar cycle (see, e.g., Hundhausen 1977). An extrapolation of this result from *ACE* at 1 AU to the position of *V1* (neglecting the small deceleration of the solar wind by the formation of pickup protons) implies that *B* decreases with increasing time, in contrast to the increasing *B* that was observed. Thus, the increase of the *B* observed by *V1* in the heliosheath from 2005.0 to 2006.9 is probably the result of the radial variation of the *B*.

This conclusion is supported by the *V2* observations from 2005.0 to 2006.92 (DOY 1–705) shown in Figure 3. During this interval, *V2* was in the supersonic solar wind, moving from 75.32 AU to 81.57 AU and from latitude S25.7° to S27.1°. A linear least-squares

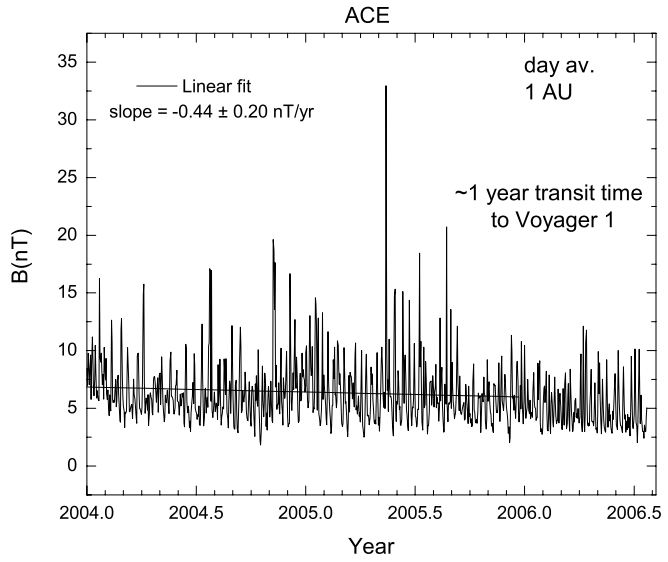


FIG. 2.—*ACE* observations of daily averages of the magnetic field strength B from 2004.0 to 2006.5. The straight line in the figure, a linear least-squares fit to the data from 2005.0 to 2006.0, has a negative slope, in contrast to the increase in B observed by *V1* during the corresponding interval displaced ~1 year later.

fit to $B(t)$ in Figure 3*a* gives a slope $s_{V2} = (-0.87 \pm 0.31) \times 10^{-5}$ nT day^{-1} $= (-0.32 \pm 0.11) \times 10^{-2}$ nT yr^{-1}. Thus, the magnetic field strength in the supersonic solar wind of the distant heliosphere was decreasing. The speed is varying with solar cycle and also with distance, owing to the formation of pickup protons (Richardson et al. 2007), but the effect of these variations are implicit in the $B(t)$ profile observed by *V2*. Since *V2* was $\approx 26^\circ$ south of *ACE*, it is likely that the decreasing B with increasing time observed by *ACE* in the ecliptic extends over at least 26° in latitude. This adds further support to the conclusion that the observation of an increase of B with increasing distance in the heliosheath by *V1* was the result of increasing distance in the heliosheath, rather than a temporal effect.

Radial variations of the speed in the heliosheath could also modify the observed profile of $B(t)$, as demonstrated by models referred to in §1 . Since the plasma instrument on *V1* is not working, we do not have measurements of the speed from a solar wind instrument. Measurements of the speed from the Low-Energy Charged Particle experiment on *V1* (R. B. Decker & S. M. Krimigis 2007, private communication) do not show a large-scale trend after day 150 (2005) but the fluctuations in speed are large.

We conclude that the limited observations to date suggest the possible existence of a large-scale increase of B with increasing distance in inner heliosheath. Since the speed of *V1* is currently 3.59 AU yr^{-1}, interpreting the observed change of B as a result of the increasing distance of *V1* implies that the radial gradient of B between 94.17 and 101.36 AU in the inner heliosheath is $(\nabla B)_{\rm IHS} \approx (0.0023 \pm 0.0011)$ nT AU^{-1}, assuming a

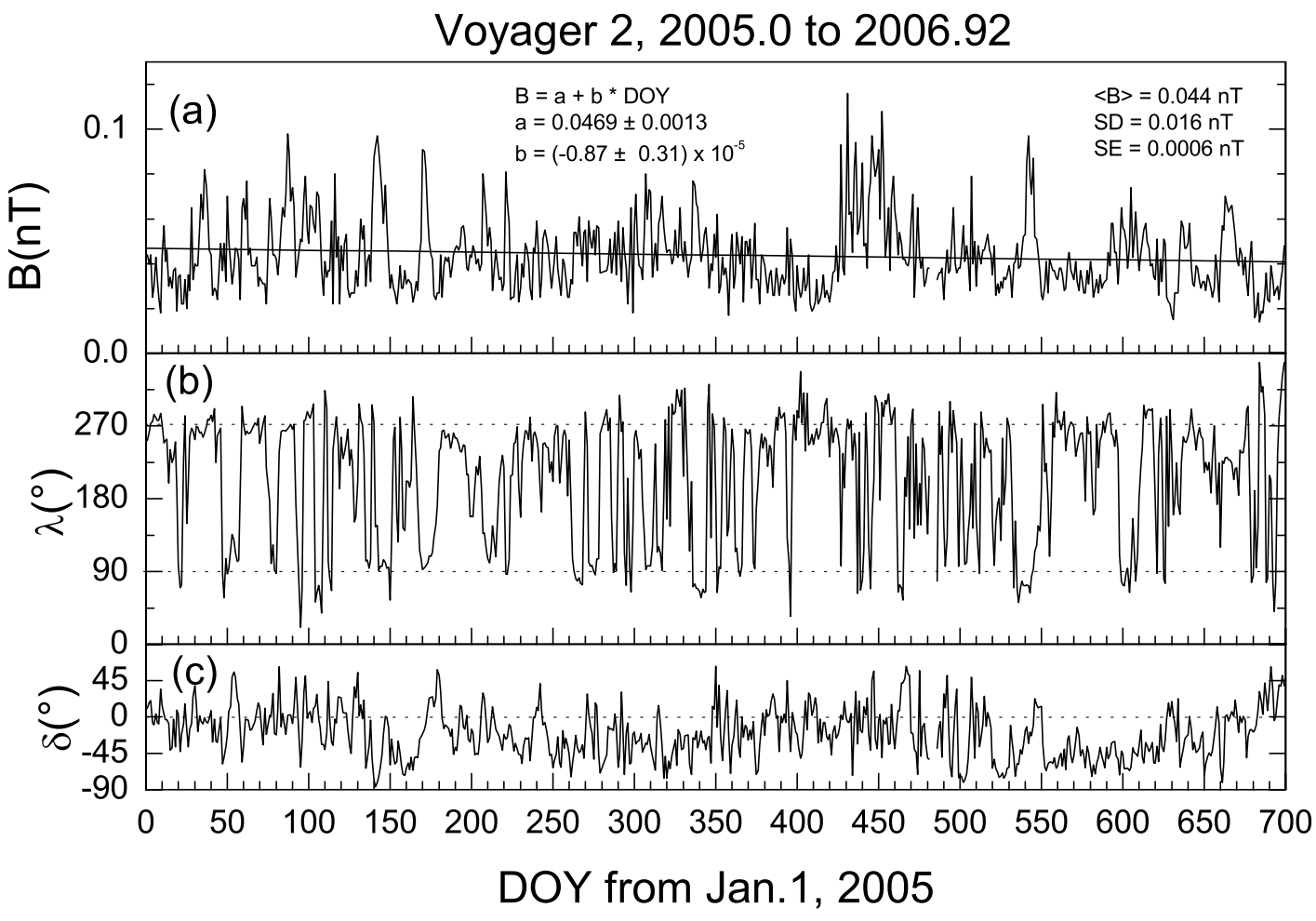


FIG. 3.—Same as Fig. 1, but for *V2*.

linear variation in the region near the TS. This variation is small, consistent with zero considering the large uncertainty related to the large fluctuations of B in the heliosheath.

The models of the heliosheath predict that the B should increase toward the heliopause, because the speed decreases from $\approx$50–100 km s^{-1} near the TS to 0 km s^{-1} at the heliopause (see, e.g., Zank 1999; Pogorelov 2006). Different models predict different profiles for the radial variation B for different positions for the heliopause. Estimates of thickness of the heliosheath in the nose direction vary depending on the interstellar magnetic field and the pressure of the interstellar plasma at the heliopause (which have not been measured directly), the model used, and the direction. Izmodenov et al. (2005) and Izmodenov & Alexashov (2006) estimate a width $\approx$52–75 AU in the direction that *V1* is moving, Opher et al. (2006) estimate a width of $\approx$55–59 AU at *V1*, and Müller et al. (2006) estimate that the ratio of the distance to the heliopause to that of TS is $\approx$1.4 in the nose direction, giving a thickness of the order of 40 AU in that direction; the thickness of the heliosheath increases away from the nose direction. Estimates of B in the heliosheath near the heliopause in the vicinity of the nose are of the order of 0.6 nT. Thus, the average radial gradient in the heliosheath $(\nabla B)_{\rm IHS}$ in the direction that *V1* is moving is expected to be of the order of $(\nabla B)_{\rm av} \approx 0.5$ nT/(50–75 AU) $\approx$ (0.007–0.010 nT AU^{-1}), which is much larger than the observed gradient $(\nabla B)_{\rm IHS} \approx (0.0023 \pm 0.0011)$ nT AU^{-1} in the region observed by *V1* behind the TS. Since there is no reason to assume a linear variation of B with R in the heliosheath, the important result is that $(\nabla B)_{\rm IHS} \approx (0.0023 \pm 0.0011)$ nT AU^{-1} provides a constraint on predictions of the gradient of B in the inner heliosheath, near the TS and far from the magnetic wall.

The difference between $(\nabla B)_{\rm IHS}$ and $(\nabla B)_{\rm av}$ confirms that the variation of B between the TS and the heliopause is not linear, as expected from the models. The observations imply that, within several AU from the TS, $(\nabla B)_{\rm IHS}$ is small compared to the average gradient in the heliosheath during the declining phase of the solar cycle, when the TS was moving toward the Sun. The model of Pogorelov (2006) predicts such an effect even in the absence of TS motion (N. V. Pogorelov 2006, private communication). The observations point to a need for more precise and comprehensive models of the radial variation of the magnetic field in the heliosheath as a function of the solar cycle, the speed of the solar wind, and the motion of the TS. We encourage the theorists to present their predictions for $B(t)$ along the trajectories of *V1* and *V2* in future publications, so that the models can be compared with present and future observations of the magnetic field in the heliosheath.

3. DISTRIBUTIONS OF MAGNETIC FIELD STRENGTH FLUCTUATIONS OBSERVED BY *V1* AND *V2*

Previous studies have shown that the distributions of B in the heliosheath are Gaussian during intervals up to 308 days (Burlaga et al. 2005, 2006b), whereas the distributions of B in the supersonic solar wind are lognormal (see, e.g., the reviews by Burlaga 1995, 2001). Let us compare the recent results for the daily averages of B shown in Figures 1 and 3 with the corresponding earlier results.

Section 2 shows that the observations of $B(t)$ by *V1* in the inner heliosheath (Fig. 1*a*) can be described as a linear trend with large fluctuations superimposed. In order to describe the distribution of the fluctuations in B, it is necessary to subtract the linear trend from the observed values of B. The subtraction gives a distribution of the fluctuations $\delta B = (B - B_{\rm linfit})$, which is shown by the points in Figure 4*a*. The solid curve in Figure 4*a* is a Gaussian fit to the distribution, and the dashed curves are the 95% confidence intervals. The distribution of the daily averages of B in the heliosheath during the 695 day interval from 2005.00 to 2006.90 (DOY 1–695) is a Gaussian distribution, consistent with earlier results.

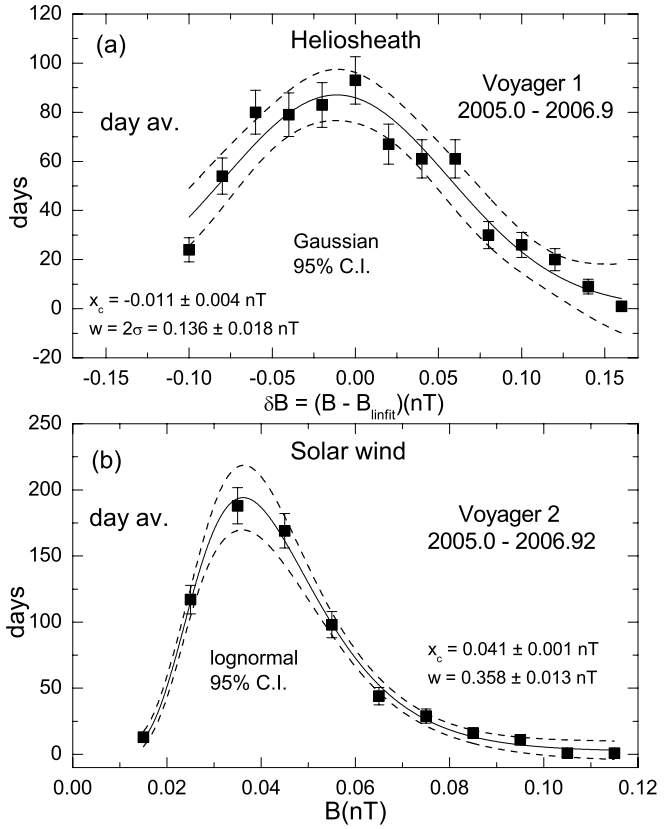


FIG. 4.—(*a*) *Squares*: Distribution of daily averages of B observed by *V1* relative to the linear trend in Fig. 1 together with a fit to a Gaussian distribution (*solid curve*) and the 95% confidence intervals (*dashed curves*). (*b*) *Squares*: Distribution of daily averages of B observed by *V2* together with a fit to a Gaussian distribution (*solid curve*) and the 95% confidence intervals (*dashed curves*). The magnetic field strength has a Gaussian distribution in the heliosheath and a lognormal distribution in the distant solar wind.

The functional form of the Gaussian distribution that was used to fit the *V1* observations in Figure 4*a* is

$$y_{\rm G} = y_o + \left[A/\sqrt{(\pi/2)}\right] w^{-1} \exp\left[-2(x - x_c)^2/w^2\right], \quad (1)$$

where $x \equiv B - B_{\rm linfit}$. The parameters of the fit are $y_o = 1 \pm 9$, $A = (15 \pm 3)$ nT, $x_c = (-0.011 \pm 0.004)$ nT, $w = 2\sigma = (0.136 \pm 0.018)$ nT, where w is 0.849 times the full width of the peak at half-height. The quality of the fit is given by the coefficient of determination $R^2 = 0.94$ and by $\chi^2/{\rm dof} = 75$. The average magnetic field strength in the 695 day interval in Figure 1*a* is $\langle B_{V1} \rangle = (0.115 \pm 0.002)$ nT, and $\sigma = (0.058 \pm 0.009)$ nT is the standard deviation of the fluctuations relative to the linear trend, giving $\sigma/\langle B_{V1} \rangle = 0.50 \pm 0.08$ for the daily averages of B in the heliosheath. The corresponding results for the shorter interval 2005 DOY 1–256 are similar: $\langle B \rangle = (0.099 \pm 0.004)$ nT, $\sigma = (0.051 \pm 0.009)$ nT, and $\sigma/\langle B \rangle = 0.52 \pm 0.09$ (Burlaga et al. 2006d).

The distribution of the daily averages of B observed by *V2* from 2005.00 to 2006.92 (DOY 1–705) in the distant supersonic solar wind is shown by the points in Figure 4*b*. The solid curve in Figure 4*b* is a fit of the data points to the lognormal distribution

$$y = y_o + \left[A/\sqrt{(2\pi)}\right](wB)^{-1} \exp\left\{-[\ln(B/B_c)]^2/(2w^2)\right\}. \quad (2)$$

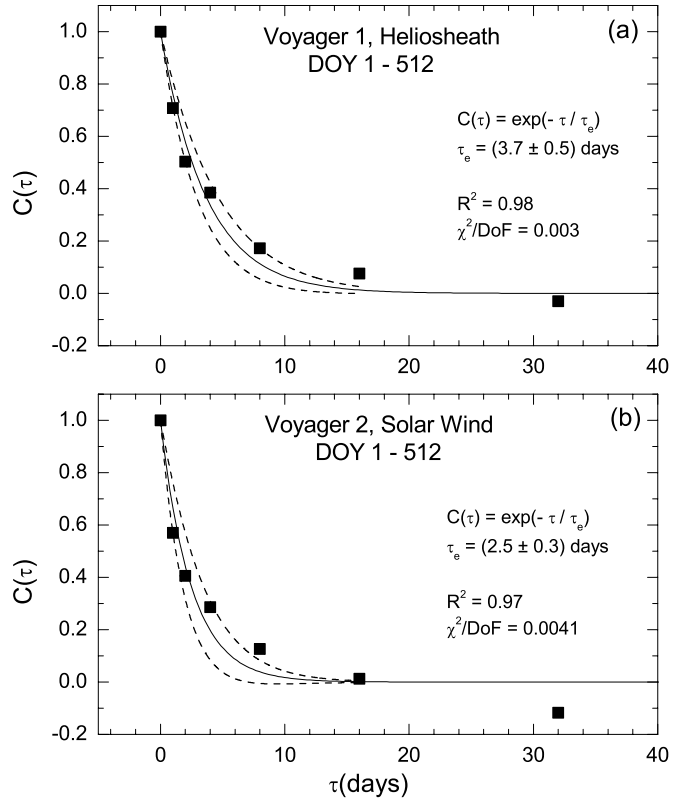


FIG. 5.—(*a*) *Squares*: Autocorrelation function of $B(t)$ observed by *V1* in the heliosheath from DOY 1–512, measured from 2005 January 1. The solid curve is an exponential fit to the observations, and the dashed curves are the 95% confidence curves. (*b*) *Squares*: Autocorrelation function of $B(t)$ observed by *V2* in the distant solar wind from DOY 1–512, measured from 2005 January 1. The solid curve is an exponential fit to the observations, and the dashed curves are the 95% confidence curves.

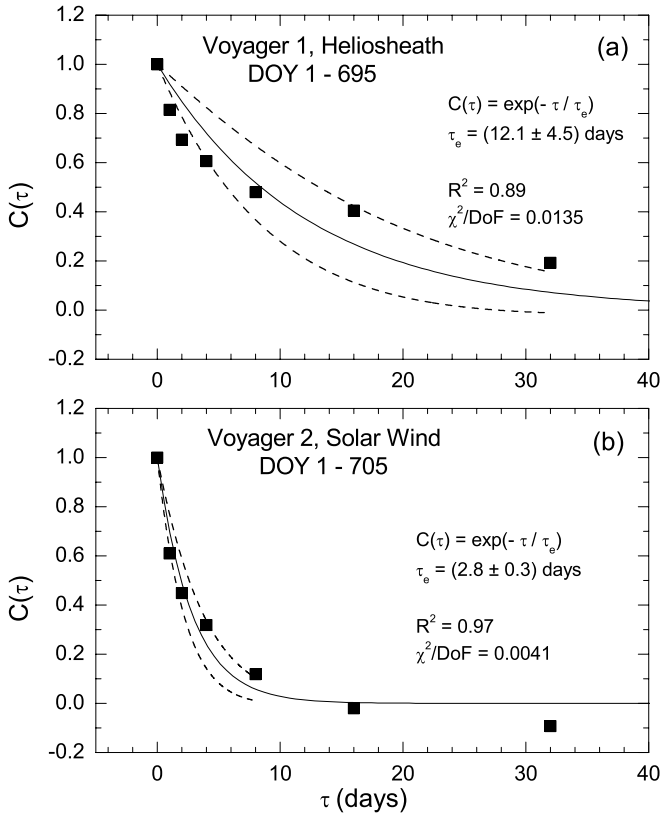


FIG. 6.—(*a*) *Squares*: Autocorrelation function of $B(t)$ observed by *V1* in the heliosheath from DOY 1–695, measured from 2005 January 1. The solid curve is an exponential fit to the observations, and the dashed curves are the 95% confidence curves. (*b*) *Squares*: Autocorrelation function of $B(t)$ observed by *V2* in the distant solar wind from DOY 1–705. The solid curve is an exponential fit to the observations, and the dashed curves are the 95% confidence curves.

The dashed curves represent the 95% confidence intervals. Inspection shows that the data are described well by the lognormal distribution, and this is confirmed by $R^2 = 0.996$ and $\chi^2/\mathrm{dof} = 30$. The parameters of this fit are $y_o = (2.1 \pm 3.2)$, $B_c = (0.0411 \pm 0.0005)$ nT, $A = (6.65 \pm 0.18)$, and $w = (0.36 \pm 0.01)$. For a lognormal distribution $w \approx \mathrm{SD}(B)/\langle B \rangle$ (Burlaga 2001), hence $\sigma/B \approx 0.36 \pm 0.01$. Thus, the relative fluctuations of daily averages of B in the heliosheath ($\sigma/B = 0.59 \pm 0.08$) are larger than those in the distant heliosphere ($\sigma/B \approx 0.36 \pm 0.01$) from 2005.0 to 2006.9.

4. CORRELATIONS OF MAGNETIC FIELD STRENGTH PROFILES OBSERVED BY *V1* AND *V2*

The daily observations of $B(t)$ are not statistically independent. There is a correlation of neighboring observations, which is measured by the autocorrelation coefficient

$$C(\tau) \equiv \langle [B(t_i + \tau) - \langle B(t_i) \rangle][B(t_i) - \langle B(t_i) \rangle] \rangle \Big/ \left\langle [B(t_i) - \langle B(t_i) \rangle]^2 \right\rangle, \quad (3)$$

where τ is a time lag. By definition, $C(\tau) = 1$ at $\tau = 0$. Typically, $C(\tau)$ is either an exponential function ($y = Ae^{(-\tau/\tau_e)}$) with a characteristic scale τ_e or a power law ($y = A\tau^{-\alpha}$) over some smaller range of scales.

During the interval DOY 1–512, the correlations measured by *V1* in the heliosheath and by *V2* in the distant supersonic solar wind are shown as a function of τ by the points in Figures 5*a* and 5*b*, respectively, which are plotted at lags $\tau_n = 2^n$, where $n = 0$, 1, 2, etc. The points were fitted with the exponential function, which is shown by the solid curves in Figures 5*a* and 5*b*; the 95% confidence limits are shown by the corresponding dashed curves. The correlation function decays exponentially, within the uncertainties, for both the *V1* and *V2* data. The decay time for the *V1* data ($\tau_e = 3.7 \pm 0.5$ days) is comparable to that for the *V2* data ($\tau_e = 2.5 \pm 0.3$ days), considering the uncertainties. The correlation decays to zero in the time $\tau_o \approx 5\tau_e$, which is (19 ± 3) days for *V1* and (12 ± 2) days for *V2*. Thus, the magnetic field strength observations are correlated over ≈half a solar rotation in both the heliosheath and the distant solar wind during the interval 1–512 days.

The correlation function measured by *V1* from DOY 1–695 [which includes the large amplitude, 200 day period sinusoidal variation of $B(t)$ discussed in § 2 in reference to Fig. 1] is significantly different from that measured by *V1* from DOY 1–512, described in the preceding paragraph. Figure 6*a* shows *V1* observations of $C(\tau_n)$ for DOY 1–695 together with the exponential fit and the 95% confidence intervals. The quality of the fit is given by $R^2 = 0.89$ and $\chi^2/\mathrm{dof} = 0.0135$. The observations marginally fall within the 95% confidence intervals, but the confidence intervals are broad compared to those in Figure 5*a*, and the points show a systematic deviation from the exponential curve in Figure 6*a*. The *e*-folding time $\tau_e = (12.1 \pm 4.5)$ days, and the correlation function decays to zero in the time $\tau_o = (60 \pm 21)$ days, much longer than the corresponding times observed in the interval DOY 1–512 (Fig. 5*a*). Evidently, the large sinusoidal variation of $B(t)$ from ≈DOY 500–695 dominates the correlation function for DOY 1–695. Thus, the correlation function is sensitive to the profile of $B(t)$,

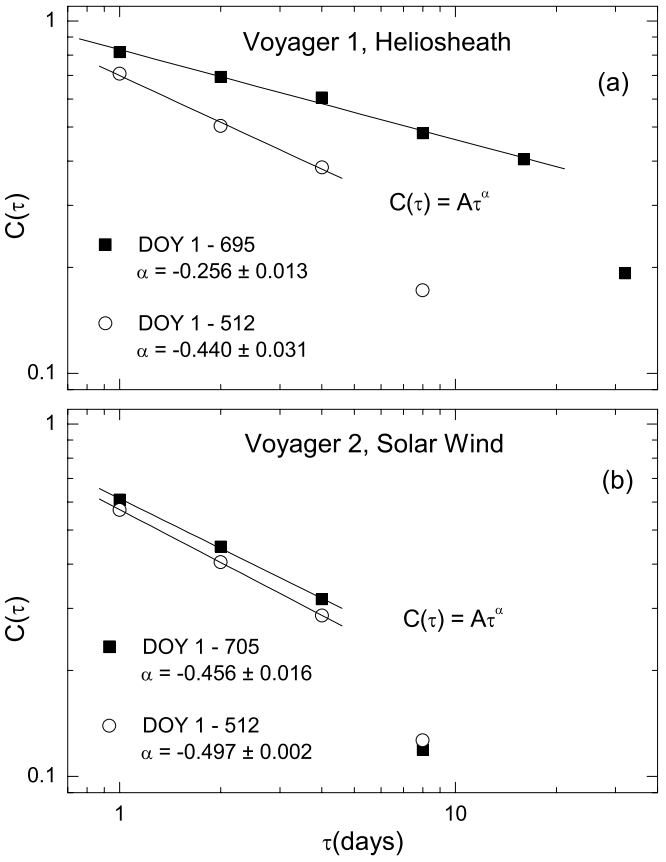


FIG. 7.—(*a*) *Squares*: Autocorrelation function of $B(t)$ observed by *V1* in the heliosheath from DOY 1–695. *Circles*: Autocorrelation function of $B(t)$ observed by *V1* in the heliosheath from DOY 1–512. The solid lines are linear fits to the observations, which are plotted on a log-log scale, indicating power laws. (*b*) *Squares*: Autocorrelation function of $B(t)$ observed by *V2* in the distant solar wind from DOY 1–705. *Circles*: Autocorrelation function of $B(t)$ observed by *V1* in the heliosheath from DOY 1–512. The solid lines are linear fits to the observations, which are plotted on a log-log scale, indicating power laws.

even though the distribution of increments of $B(t)$ is not (as shown in § 5).

The correlation function measured by *V2* during the interval DOY 1–705 is shown in Figure 6*b*, together with an exponential fit. The exponential fit describes the observations of $C(\tau)$ rather well ($R^2 = 0.97$ and $\chi^2/\mathrm{dof} = 0.004$). The decay time observed by *V2* from DOY 1–705 ($\tau_e = 2.8 \pm 0.3$ days) is the same as that observed by *V2* from DOY 1–512 ($\tau_e = 2.5 \pm 0.3$ days). The corresponding times to decay to zero are $\tau_o = (14 \pm 2)$ days and $\tau_o = (13 \pm 2)$ days, respectively.

Under some conditions in the solar wind the correlation function for daily averages of $B(t)$ is a power law over some range of scales (Burlaga & Viñas 2005a). Figure 7 shows the correlation functions discussed above on a log-log scale. Figure 7*a* shows $C(\tau)$ for the heliosheath observations of *V1* from DOY 1–695 (*squares*) and from DOY 1–512 (*circles*). The observations for the larger interval can be fit with a straight line over the range $1 \leq \tau \leq 16$ days, indicating a power law $C(\tau) = \tau^{\alpha}$ ($\alpha = -0.256 \pm 0.013$). The observations for the shorter interval can be fit with a straight line over the more limited range $1 \leq \tau \leq 4$ days, indicating a power law $C(\tau) = \tau^{\alpha}$ ($\alpha = -0.440 \pm 0.031$). It is surprising to observe that the larger interval, which contains the large sinusoidal variation of B from DOY 513–695, has a power-law correlation function over a relatively wide range of lags.

Figure 7*b* shows $C(\tau)$ for the *V2* solar wind observations from DOY 1–705 (*squares*) and from DOY 1–512 (*circles*). The observations for both intervals can be fit with a straight line over the limited range $1 \leq \tau \leq 4$ days, indicating a power law $C(\tau) = \tau^{\alpha}$ ($\alpha = -0.469 \pm 0.013$). The observations for the shorter interval indicate a power law $C(\tau) = \tau^{\alpha}$ ($\alpha = -0.497 \pm 0.002$). It is significant that the *V2* observations give the same exponent α for both time intervals. Moreover, the α observed by *V2* in the solar wind is the same (within the uncertainties) as that observed by *V1* in the heliosheath from DOY 1–512 ($\alpha = -0.440 \pm 0.031$). It is possible that the common values of α are coincidental. Another possibility is that the TS does not significantly change the correlation function of $B(t)$, even though it alters the distribution of B from lognormal to Gaussian. We cannot demonstrate this invariance, because *V2* was not upstream of *V1*. This possibility should be investigated with magnetohydrodynamic (MHD) models.

5. DISTRIBUTIONS OF INCREMENTS OF MAGNETIC FIELD STRENGTH OBSERVED BY *V1* AND *V2*

It has been shown that the distribution of increments of daily averages of B, $dB0(t_i) \equiv B(t_i + 1\ \mathrm{day}) - B(t_i)$ in the heliosheath (Burlaga et al. 2006d) and in the supersonic solar wind (Burlaga & Viñas 2005a, 2005b), is the distribution that was introduced by Tsallis (1988) in the context of nonextensive statistical mechanics. The daily observations of $dB0$ measured by *V1* from 2005.00 to 2006.90 and by *V2* from 2005.00 to 2006.92 are shown in Figures 8*a* and 8*b*, respectively. Both time series show an intermittent, spiky character of $dB0(t_i)$. The distributions of $dB0$ for *V1* and *V2* are shown by the points in Figures 9*a* and 9*b*, respectively. The curves in Figures 9*a* and 9*b* are the fits of these observations to the symmetric Tsallis distribution

$$y_{\mathrm{T}} = A\left[1 + (q-1)\beta x^2\right]^{-1/(q-1)}. \tag{4}$$

The Tsallis distribution is a generalization of the Boltzmann-Gibbs (B-G) distribution. In the limit $q \rightarrow 1$, the Tsallis distribution is the B-G distribution with $x^2 =$ energy E. The tails of the Tsallis distribution are increasingly larger than those of the B-G distribution as q increases. The parameter q is introduced in the definition of entropy for nonextensive systems; the entropy of two parts of a system is not the sum of the entropy of the parts when $q \neq 1$, which is a property of nonlinear, multifractal systems such as the solar wind. Intermittency (spikiness with a certain scaling symmetry) in signals such as those measured in small-scale turbulence and in features observed at larger scales in the solar wind can be described accurately by the Tsallis distribution, but not by the B-G distribution of ordinary statistical mechanics.

Parameters of the fit for the *V1* data in the heliosheath from DOY 1–695 to equation (3) are $A = 0.304$, $\beta = 1153$, and $q = 1.52 \pm 0.03$. The corresponding parameters of the fit for the *V2* data in the supersonic solar wind from DOY 1–705 are $A = 0.342$, $\beta = 5426$, and $q = 1.48 \pm 0.04$. Both a visual inspection of Figure 9 and the value $R^2 = 0.99$ measuring the quality of the fit for both *V1* and *V2* indicate that the Tsallis distribution provides an excellent fit to both the *V1* and *V2* observations. The nonextensivity parameter q for the *V1* observations of $dB0$ in the heliosheath is essentially the same as that for the *V2* observations of $dB0$ in the distant supersonic solar wind, viz., $q \approx 3/2$.

Since the fluctuations in $B(t)$ observed by *V1* from DOY 500–695 in Figure 1 contain a very large feature that was not observed among the fluctuations from DOY 1–512, we computed the distribution of $dB0$ for the daily averages of B in the interval DOY 1–512. This distribution (not shown) is nearly identical to that in Figure 5*a*. A fit of the distribution of $dB0$ for the 512 day interval to the Tsallis distribution gives $A = 0.289 \pm 0.026$,

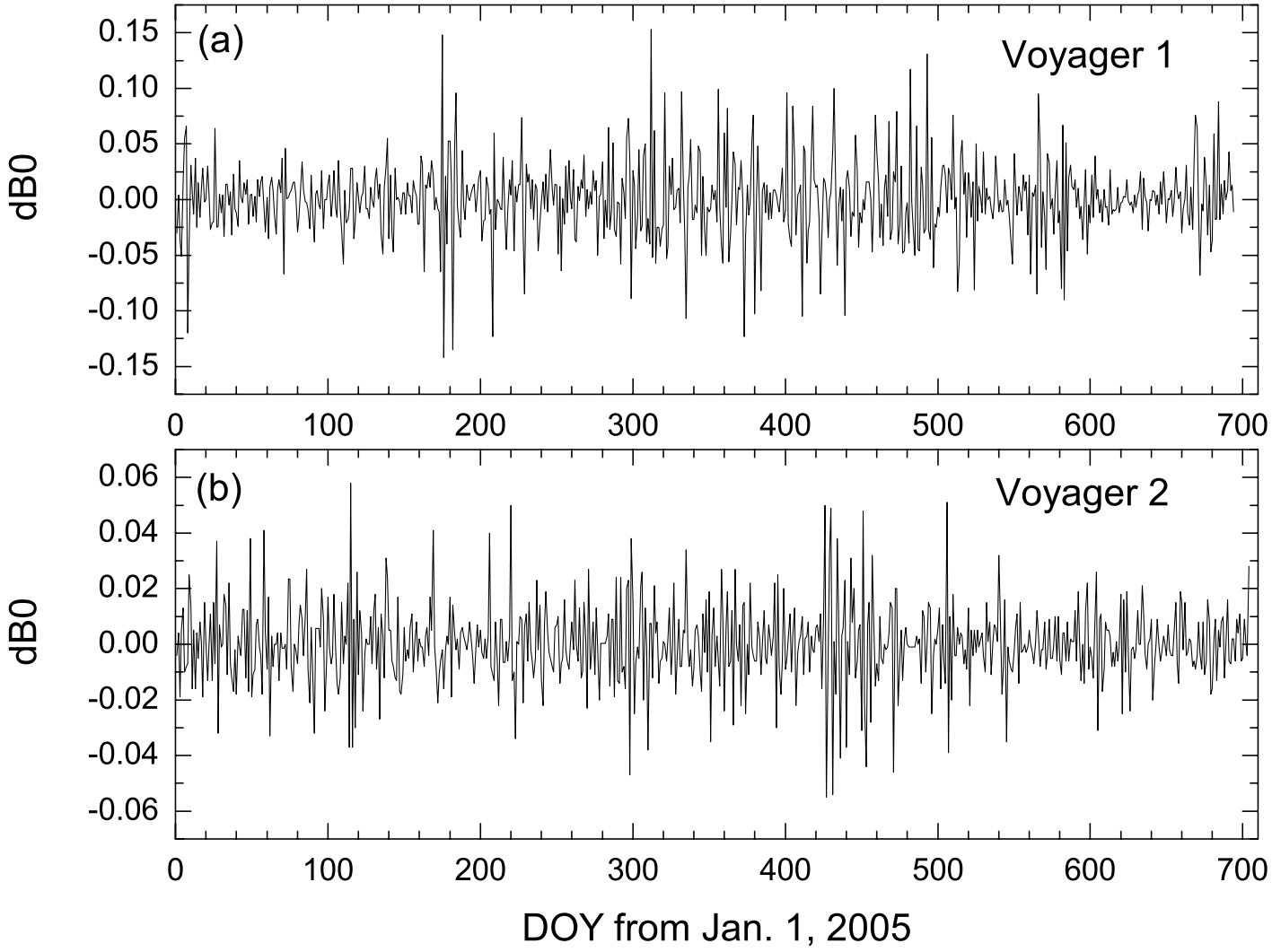


FIG. 8.—(*a*) Increments of daily averages of *B* observed by *V1* from DOY 1–695. (*b*) Increments of daily averages of *B* observed by *V2* from DOY 1–705.

$\beta = 1075 \pm 350$, and $q = 1.55 \pm 0.05 \approx 3/2$, consistent with that derived for the 695 day interval ($q = 1.52 \pm 0.03$). The quality of the fit is given by $R^2 = 0.98$ and $\chi^2/\mathrm{dof} = 0.0074$. Thus, the unusual sinusoidal feature in $B(t)$ observed during the last 200 days of the interval in Figure 1*a* does not significantly change either the nonextensivity parameter q or the width of the Tsallis distribution.

Inspection of Figure 9 shows that the distribution of $dB0$ in the heliosheath is wider than that in the solar wind during the corresponding time interval. The average B in the heliosheath observed by *V1* from 94.17 to 101.36 AU ($\langle B_{V1} \rangle = -0.155$ nT) is 3.5 times larger than that observed in the distant solar wind by *V2* from 75.3 to 81.57 AU (0.044 nT). The width of a Tsallis distribution is inversely related to the parameter β. The ratio $(1/\beta_{V1})/(1/\beta_{V2}) = 5426/1153 = 4.7$. The variation of B relative to $\langle B \rangle$ observed in the heliosheath by *V1* is 30% greater than observed in the distant solar wind by *V2*.

6. DISTRIBUTIONS OF THE MAGNETIC FIELD DIRECTIONS OBSERVED BY *V1* AND *V2*

6.1. *Distributions of Elevation Angles*

The distribution of daily averages of the elevation angle δ of B in HG coordinates measured by *V1* in the heliosheath from 2005.0 to 2006.9 is shown in Figure 10*a*. The average of the δ-distribution is $\langle \delta \rangle = 1^\circ$, and the standard deviation (SD) is $\approx 30^\circ$. The distribution of daily averages of δ measured by *V2* in the distant heliosphere between $R = 94.17$ and 101.36 AU during the interval from 2005.0 to 2006.92 are shown in Figure 10*b*. The average of the δ-distribution is $\langle \delta \rangle = -20^\circ$, and the SD of δ is 31°. The distribution of δ for *V1* measurements is skewed toward the left, while that for *V2* is skewed toward the right.

Both systematic and random errors contribute to the uncertainties of the measurements of the components of $\boldsymbol{B}$ and hence the angles. It is not possible to compute the uncertainties of the angles rigorously, since the systematic errors can only be estimated indirectly in some average sense. Since angles are computed from the components of the magnetic field using several arithmetic and trigonometric calculations, the uncertainties in the angles are larger than those of the components. The uncertainties in the angles are large (of the order $\pm 45^\circ$ for δ) when B is weak (<0.05 nT) and even larger when δ is large (which is difficult to determine because of the uncertainties in δ). Since the uncertainties in the components measured by *V2* are larger than those for *V1*, the uncertainties of the angles measured by *V1* are larger than those measured by *V2*. The differences between the distributions of δ for *V1* and *V2* (shown in Figs. 3*a* and 3*b*, respectively) can be attributed to the uncertainties in the measurements of the angles.

One significant result in Figure 10 is that the widths of the distributions of δ measured by the SDs are $\approx 30^\circ$ for both *V1* and *V2*. Since the uncertainties in computing the angles contribute

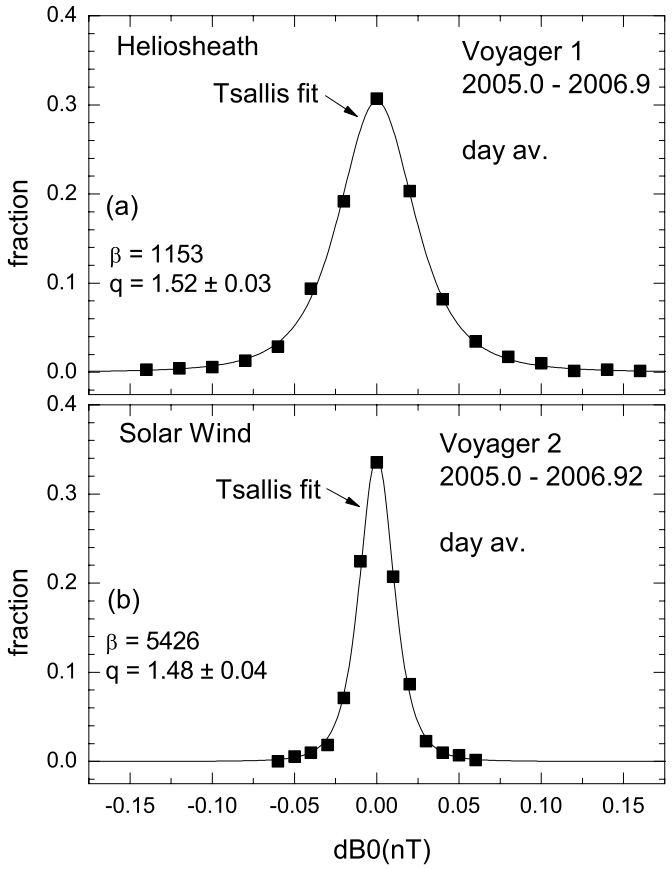


FIG. 9.—(*a*) *Squares*: Observed distribution of increments of B ($dB0$) observed by *V1* in the heliosheath from DOY 1–695. *Solid curve*: Fit of the Tsallis distribution to the observations. (*b*) *Squares*: Observed distribution of increments of B ($dB0$) observed by *V2* in the distant solar wind from DOY 1–705. *Solid curve*: Fit of the Tsallis distribution to the observations. The nonextensivity parameter q is $\approx 3/2$ for both data sets.

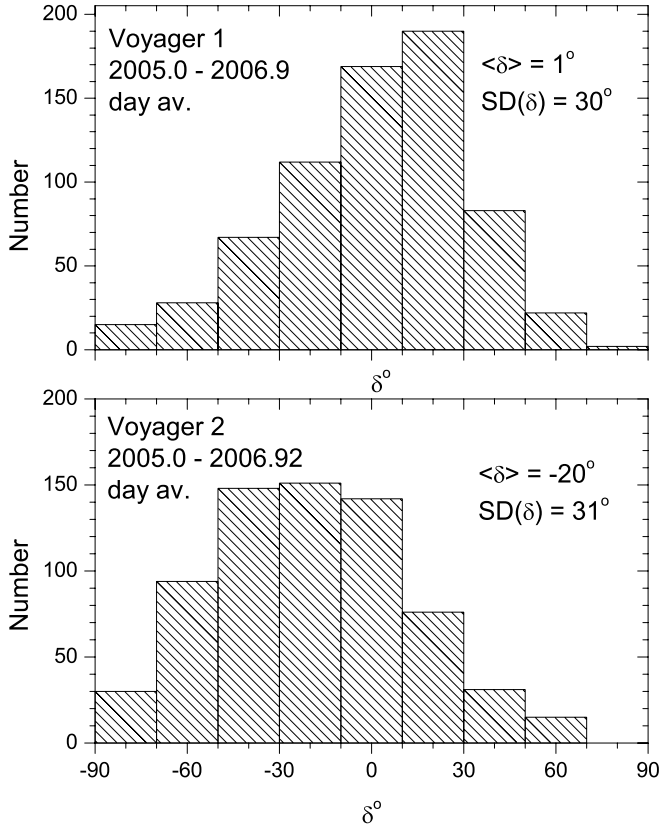


FIG. 10.—(*a*) Daily averages of the elevation angle δ observed by *V1* from DOY 1–695. (*b*) Daily averages of the azimuthal angle δ observed by *V2* from DOY 1–705.

significantly to the widths of the distributions, we can conclude that the SD of the fluctuations of daily averages of δ is $<30^\circ$.

6.2. *Sectors and Distributions of Azimuthal Angles*

Figures 11*a* and 11*b* show daily averages of the azimuthal angle λ of $\boldsymbol{B}$ in HG coordinates as a function of DOY for $\approx$700 days from the beginning of 2005 for *V1* and *V2*, respectively. A sector pattern (Ness & Wilcox 1964; Smith 2001; Ness & Burlaga 2001) is evident in the *V1* data, although the pattern changes with time. Individual sectors are highly distorted by dynamical processes in the solar wind beyond several AU (Behannon et al. 1989; Burlaga 1995) and in the heliosheath (e.g., Jokipii 2005). Nevertheless, the relative fraction of positive and negative polarities is determined primarily by the position of the spacecraft relative to the latitudinal extent of the heliospheric current sheet (HCS), rather than by the dynamical processes that stretch and squeeze sectors, since magnetic flux is conserved. Both positive and negative polarities for λ are observed in the *V2* data, but the sector pattern is less clear than in the *V1* data. The two continuous curves in Figure 11 are 200 day running averages of the profiles of λ versus time for *V1* and *V2*. For the *V1* data in the heliosheath, the curves show a trend from "away" polarity at the beginning of 2005 to "toward" polarity near the end of the interval. No such trend is observed in the *V2* data for the supersonic solar wind.

Another way to view the evolution of the polarities of the *V1* data in the heliosheath is to divide the 695 day interval into three equal parts and compute distributions of λ for each of the three intervals. These distributions are shown in Figure 12. Early in the interval, from DOY 1–232, the distribution is double peaked, with maxima near the Parker spiral angles $\lambda = 90^\circ$ and 270°, but the peak corresponding to the away polarities is strongly dominant. This peak is largely due to the exceptionally long-lasting sector that was observed shortly after *V1* crossed the TS into the heliosheath. It has been shown (Jokipii 2005; E. C. Stone 2005, private communication) that this unusually long sector is simply a consequence of a normal heliospheric sector moving at unusually slow speeds, comparable to the spacecraft speed (17 km s^{-1}) in the subsonic heliosheath, as a result of the sunward motion of the TS (Whang et al. 2004). In the second third of the interval, from DOY 233–464, there are again two peaks near the spiral field angles, but now the peaks are comparable to one another. In the third interval, from DOY 465–695, there is a single peak corresponding to "toward" polarity.

In the case of the *V2* data in the interval from DOY 1–705, the continuous curve in Figure 12*b* shows no trend of λ versus time, so we compute a single distribution of λ for the entire interval. This distribution of λ (shown in Fig. 13) has two peaks (near the spiral angles $\lambda = 90^\circ$ and 270°), but the dominant peak corresponds to "away" polarity. The ratio of the areas of the two peaks of the λ-distribution in Figure 13 is $A_2/A_1 = (8407 \pm 740)/(5573 \pm 952) = 1.5 \pm 0.3$; 60% of the flux is pointing away from the Sun and 40% is pointing toward the Sun.

A possible interpretation of the preceding results for the polarity distributions of the *V1* and *V2* data is shown by the illustration in Figure 14. The wavy curve is a highly simplified schematic representation of the intersection of a meridional plane and the HCS (Schulz 1973; Schatten et al. 1969; Hundhausen 1972; Burlaga 1995; Smith 2001) assuming a latitudinal extent of $+35^\circ$ in the

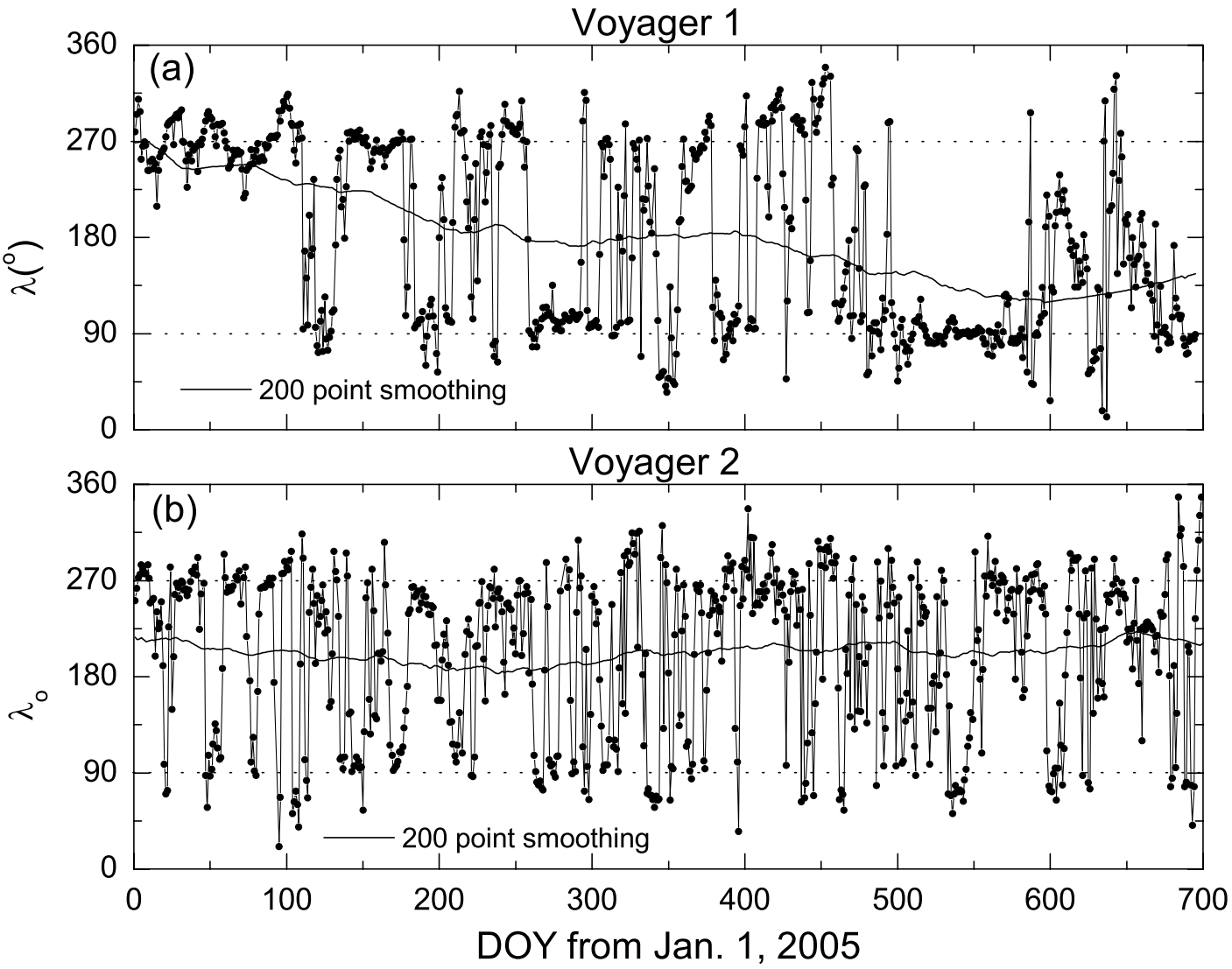


FIG. 11.—(*a*) *Points*: Daily averages of the azimuthal angle δ observed by *V1* from DOY 1–695. The solid curve, derived by 200 point running averages, shows a trend from predominantly positive polarities ($\approx 270^\circ$) at the beginning of the interval to mixed polarities ($\approx 180^\circ$) in the middle of the interval to predominantly negative polarities ($\approx 90^\circ$) near the end of the interval. (*b*) *Points*: Daily averages of the azimuthal angle δ observed by *V2* from DOY 1–705. The solid curve, derived by 200 point running averages, shows no tendency for polarity to change across the interval. Both positive and negative polarities were observed by *V2*, with an excess of positive polarities.

northern hemisphere and -35° in the southern hemisphere. The position of *V2* at 2007.0 (radial distance = 101.36 AU and latitude N34.2°) is shown by the plus sign just beyond TS, which is drawn as a circle at 95 AU. The position of *V2* at 2007.0 (radial distance $R = 81.57$ AU; latitude S27.1°) is shown by the cross inside the TS. During the interval from ≈2005.0 to 2007.0 the latitudinal extent of the HCS was decreasing. If the HCS extended beyond the latitude of *V2* from 2005–2007, as shown in Figure 14, then *V2* would be within the sector zone (Burlaga & Ness 1996, 1998) measuring both positive and magnetic polarities with nearly equal probability throughout the 705 day interval, as observed (Fig. 13). If the maximum latitudinal extent of the HCS were just below the latitude of *V1* during the last third of the interval DOY 1–695 (as illustrated in Fig. 14) then *V1* would observe predominately positive polarity during the interval, as observed (Fig. 12*c*). We shall now show that the latitudinal extent of the HCS was such that the interpretation of the *V1* and *V2* observations of the distribution of λ in terms of the sketch in Figure 14 is probably valid.

The HCS is a surface that encircles the Sun, separating positive and negative magnetic polarities of the Sun. If the magnetic axis of the Sun were a dipole aligned with the rotation axis, then the surface would be a plane coincident with the solar equatorial plane; the intersection of such a plane with a spherical surface with a radius of $\approx 2\ R_\odot$ ("the source surface ") is a circle. In general, the magnetic axis of the Sun (insofar as it can be defined) is effectively tilted with respect to the solar rotation axis (Smith 2001), and the intersection of the HCS with the source surface (the " neutral line") is a sinusoidal curve whose amplitude is related to the tilt angle. This amplitude varies with the solar cycle (see, e.g., Hundhausen 1977), being large the near solar maximum and small near the solar minimum (see, e.g., Burlaga & Ness 1997). In general, there are north–south asymmetries (Burlaga et al. 1981; Smith et al. 2000) and additional distortions to the HCS owing to coronal holes (Burlaga 1995; Bruno et al. 1982) and transient phenomenon on the Sun (Villante et al. 1979).

It is possible to compute the neutral line on the source surface from observations of the photospheric magnetic field (Altschuler & Newkirk 1969; Schatten et al. 1969). Various models have been published, but the most widely used model is that described by Hoeksema (1991, 1995), which is implemented using observations from the Wilcox Solar Observatory. Hoeksema computes

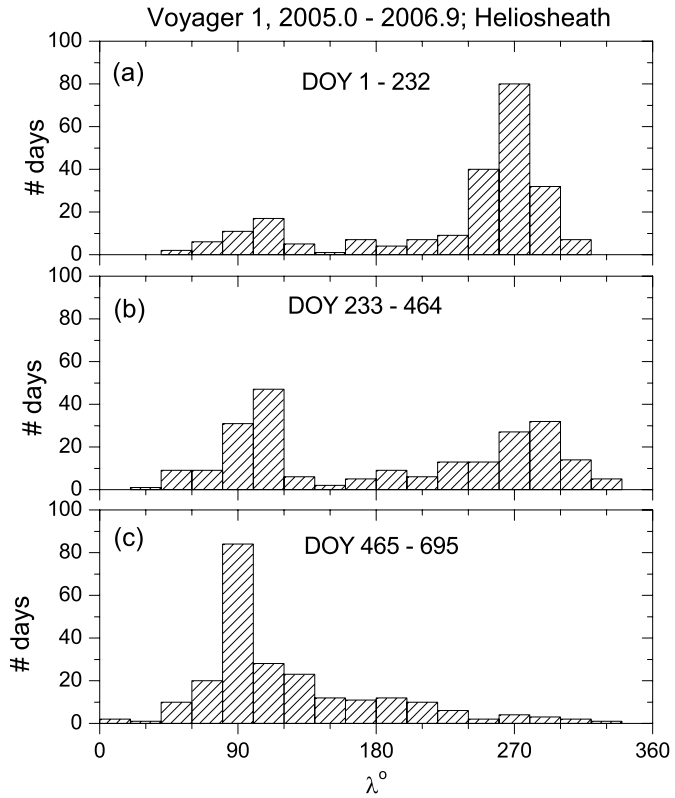


FIG. 12.—(*a*) Distribution of λ observed by *V1* from DOY 233–464, showing predominantly positive polarity. (*b*) Distribution of λ observed by *V1* from DOY 1–232, showing both positive polarities. (*c*) Distribution of λ observed by *V1* from DOY 465–695, showing predominantly negative polarity.

the maximum and minimum latitudinal extent (θ_M and θ_m, respectively) of the neutral line on the source surface for each solar rotation as a function of time, and he posts the results online.[4]

Since the HCS is carried radially away from the Sun with the solar wind, θ_M and θ_m are approximately the same throughout the solar wind, to the extent that the neutral line is stationary during the propagation time. Hoeksema (1991, 1995) presents the results of two different models, the "classical model" and the "radial model" (Wang and Sheeley 1992), which predict different results

[4] See Web site at http://wso.stanford.edu/.

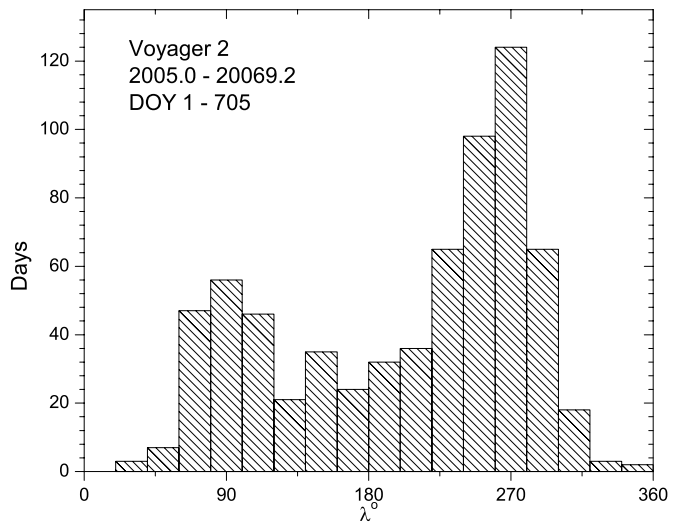


FIG. 13.—Distribution of λ observed by *V2* from DOY 1–705, showing predominantly positive polarity, with maxima in the spiral field directions, 90° and 270°.

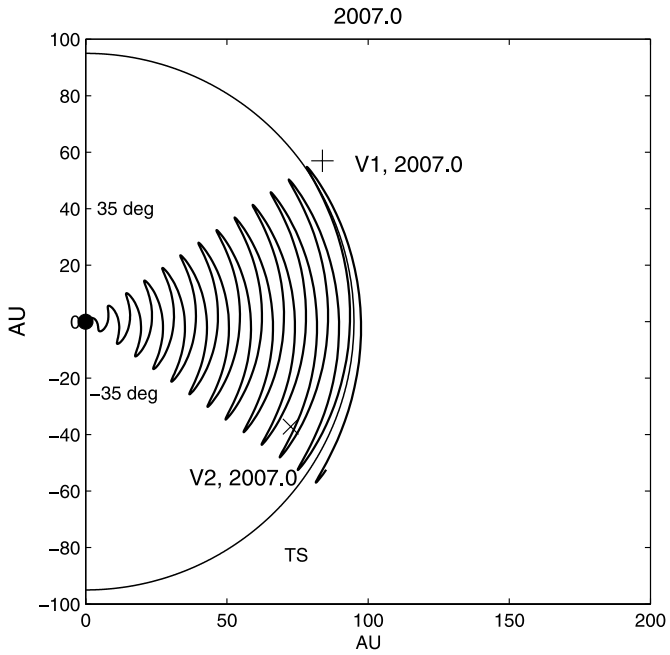


FIG. 14.—Illustration of the relationship between the HCS and the positions of *V1* and *V2* for the case that the tilt angle (maximum latitudinal extent of the HCS) is 30°. The HCS is illustrated in a highly schematic fashion by the wavy curve, which represents the intersection of the HCS surface with a meridional plane. The points show the positions of *V1* and *V2* at 2007.0.

for θ_M and θ_m. Generally, the observations are more consistent with the classical model. Observations from *Ulysses* at less than or equal to 5 AU (Balogh & Smith 2001; Smith et al. 1978, 1988, 1993, 2001) and from *V1* and *V2* (Burlaga & Ness 1993, 1997; Burlaga et al. 2002) confirm that one can predict the latitudinal extent of the HCS from the source surface model and solar magnetic observations.

Figure 15 shows the classical model predictions of θ_M and θ_m as a function of time from 1985.0 to 2007.0. Figure 15 also shows the latitudes of the trajectories of *V1* and *V2* from 1996 through

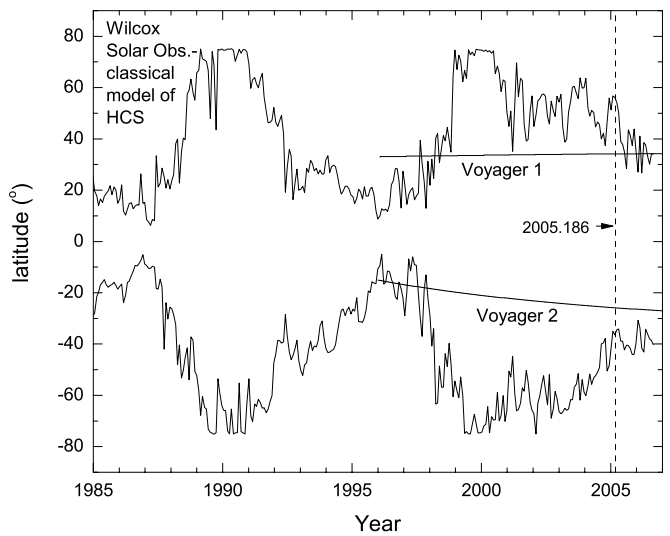


FIG. 15.—Maximum and minimum latitudinal extent of the HCS, assumed equal to the maximum and minimum latitudinal extent of the neutral line on a source surface at 2.5 $R_\odot$ for each Carrington rotation for the years 1985.0–2007.0, computed with the "classic" model using the solar magnetic field observations from the Wilcox Solar Observatory. The smooth curves are the latitudes of the trajectories of *V1* and *V2*. The vertical dashed line is that time at which *V1* observed a transition to uniform polarity, projected back in time to the source surface.

2006. There is an overall decline in the amplitude of the HCS from solar maximum in the year 2000 to 2006. When the maximum latitudes of the HCS drop below the latitudes of the *V1* and *V2*, one expects to observe a constant polarity of the magnetic field corresponding to the polarity of the northern and southern polar regions of the Sun, respectively. Figure 15 shows that the latitude of the HCS has been higher than that of *V2* since 1998, including the years 2005 and 2006, which are the subject of this paper.

Thus, it is predicted that *V2* should observe both positive and negative polarities during the years 2005 and 2006, as observed (see Fig. 13). On the other hand, Figure 15 shows that the latitude of the HCS began to drop below the latitude of *V1* at ≈2005.186, indicated by the vertical dashed line in the figure. A similar effect (with the opposite polarity) was observed by *V1* at N32° and by *Ulysses* at S30° during 1993 in the declining phase of the previous solar cycle (Burlaga & Ness 1996, 1997). One expects *V1* to observe predominately negative magnetic polarities beginning approximately 1 year after this date, allowing for the propagation time of the solar wind from the source surface to the position of *V1*.

With a reasonable estimate of the mean solar wind speed, a projection of the neutral line along the radial direction from the footprint of the HCS to *V1* predicts that the transition in polarities would arrive at *V1* at approximately 2006.364, which is marked by the vertical dashed line in Figure 1. Figure 1 shows that *V1* observed an extended region of negative polarity for nearly 100 days after that time, and highly variable directions for the remainder of the interval to DOY 695. (The variable directions were observed when B was weak, so the variability might be largely due to the result of uncertainties in determining the angles). Thus, the *V1* observations and the extrapolations of the source surface computed by Hoeksema (1991, 1995) suggest that the latitude of the HCS was moving below the latitude of *V1* after approximately 2006 DOY 135. If this is the case, we expect that *V1* will observe predominantly negative polarities during 2007 and 2008.

7. DISCUSSION AND SUMMARY

We analyzed daily averages of the magnetic field $\boldsymbol{B}$ observed by *V1* in the 695 day interval from 2005.00 to 2006.90 (DOY 1–695, when *V1* was in the heliosheath) and by *V2* in the 705 day interval from 2005.00 to 2006.92 (DOY 1–705, when *V2* was in the supersonic solar wind). The relatively long intervals considered allow us to describe both a possible large-scale trend of the magnetic field strength B in the heliosheath and the large-scale fluctuations about the trend. A unique large sinusoidal structure with amplitude ≈0.12 nT and period ≈200 days was observed by *V1* from ≈DOY 500 to 705. We also determined the variations of the magnetic polarity observed by *V1* near N34° and *V2* near S26°.

V1 observed a small increase in B during the 695 day interval in the heliosheath. A least-squares fit gives a linear increase of B versus time, with a slope of $s_{V1} = (2.31 \pm 1.09) \times 10^{-5}$ nT day^{-1} = (0.0084 ± 0.0040) nT yr^{-1}. A similar fit of the *ACE* observations during the corresponding interval (from 2004.0 to 2006.5) shows the opposite trend, a linear decrease of B versus time with $s_{ACE} = (-0.44 \pm 0.20)$ nT yr^{-1}. Decreasing B with increasing time is expected during the declining phase of the solar cycle under consideration. *V2* also observed a decrease in B with increasing time, with $s_{V2} = (-0.87 \pm 0.31) \times 10^{-5}$ nT day^{-1} = $(-0.32 \pm 0.11) \times 10^{-2}$ nT yr^{-1}. Since *V2* was ≈26° south of *ACE*, the decreasing B with increasing time observed by *ACE* extends over at least 26° in the latitude. We conclude that increase of the B versus observed by *V1* in the heliosheath is probably the result of the radial variation of the B, rather than a temporal effect.

Since the speed of *V1* is currently 3.59 AU yr^{-1}, interpreting the observed change of B as a result of the increasing distance of *V1* implies that the radial gradient of B between 94.17 and 101.36 AU in the inner heliosheath close to the TS is $(\nabla B)_{\rm IHS} \approx (0.0023 \pm 0.0011)$ nT AU^{-1}. The average radial observed by *V1* is much smaller than the average radial gradient $(\nabla B)_{\rm av} \approx 0.5$ nT/(50−75) ≈ (0.007 ± 0.010) nT AU^{-1} that is expected in the heliosheath in the direction of *V1*. The difference between $(\nabla B)_{\rm IHS}$ and $(\nabla B)_{\rm av}$ implies that, within several AU from the TS, $(\nabla B)_{\rm IHS}$ was small compared to the average gradient between the TS and heliosheath. This conclusion applies to the declining phase of the solar cycle. The observations point to a need for more precise and comprehensive models of the radial variation of the magnetic field in the heliosheath as a function of the solar cycle, with consideration of motion of the TS.

Previous studies have shown that the distributions of fluctuations of B in the heliosheath are Gaussian during intervals up to 308 days, while those in the supersonic solar wind are lognormal. We found that the distribution of the daily averages of B in the heliosheath during the 695 day interval from 2005.00 to 2006.90 is a Gaussian distribution (relative to the linear trend), consistent with earlier results. However, the relative width of the Gaussian fit in the interval 2005.00–2006.90 [$\sigma/\langle B_{V1}\rangle = (0.058 \pm 0.009)/(0.115 \pm 0.002) = 0.50$] is similar to that for a shorter earlier interval, 2005.00–2005.70 ($\sigma/\langle B_{V1}\rangle = 0.52$).

The distribution of the daily average magnetic field strengths observed by *V2* in the distant supersonic solar from 2005.00 to 2006.92 was lognormal, with $w = (0.36 \pm 0.01)$. The observed fluctuations in daily averages of B in the heliosheath ($\sigma/\langle B_{V1}\rangle = 0.050 \pm 0.08$) are larger than those in the distant heliosphere ($\sigma/\langle B_{V2}\rangle = 0.036 \pm 0.01$) from 2005.00 to 2006.92.

The autocorrelation function $C(\tau)$ of $B(t)$ measured by *V1* in the heliosheath during the interval DOY 1–695 (DOY 1–512) is approximately an exponential function with an e-folding time $\tau_e = 12.1 \pm 4.5$ days ($\tau_e = 3.7 \pm 0.5$ days). The e-folding time of the autocorrelation function measured by *V1* from DOY 1–695 is significantly different for the two intervals, because of a large-amplitude "sinelike" variation in $B(t)$ with a period of ≈200 days from ≈DOY 500 to 695. The time for $C(\tau)$ to decay to zero is $\tau_o \approx 5\tau_e$, which is ≈60.5 days (≈19 days) for the two intervals.

The autocorrelation function $C(\tau)$ of $B(t)$ measured by *V2* in the distant supersonic solar wind during the interval DOY 1–705 (DOY 1–512) is also approximately an exponential function. The decay time observed by *V2* from DOY 1–705 ($\tau_e = 2.8 \pm 0.3$ days) is the same as that observed by *V2* from DOY 1–512 ($\tau_e = 2.5 \pm 0.3$ days). The correlation function decays to zero in $\tau_o \approx 5\tau_e \approx$ 13 days, ≈one-half of a solar rotation.

The correlation function $C(\tau)$ for the heliosheath observations of $B(t)$ by *V1* from DOY 1–695 is a power law τ^α with $\alpha = -0.256 \pm 0.013$ in the range $1 \le \tau \le 16$ days. On the other hand, $C(\tau)$ from DOY 1–512 is a steeper power law ($\alpha = -0.440 \pm 0.031$) over the more limited range $1 \le \tau \le 4$ days. It is notable that the longer interval, which contains the large sinusoidal variation of B from DOY 513–695, has a power-law correlation function over a wider range of lags than the shorter interval.

The correlation function $C(\tau)$ for the distant supersonic solar wind observations of $B(t)$ by *V2* from DOY 1–705 (DOY 1–512) is a power law τ^α with $\alpha = -0.469 \pm 0.013$ ($\alpha = -0.497 \pm 0.002$) in the range $1 \le \tau \le 4$ days. The α observed by *V2* in the solar wind is the same (within the uncertainties) as that observed by *V1* in the heliosheath from DOY 1–512 ($\alpha = -0.440 \pm 0.031$). It is possible that the TS does not significantly change the correlation function of $B(t)$, even though it alters the distribution of B

from lognormal to Gaussian. This possibility should be investigated with MHD models.

Although the distribution of fluctuations in B in the heliosheath is Gaussian, the time profile $B(t)$ shows a filamentary structure with jumps in B, some of which are large compared to the mean magnetic field strength. The changes in daily averages of B are described by the increments $dB0 \equiv B(t + 1 \text{ day}) - B(t)$. The distribution of daily observations of $dB0$ measured by *V1* from DOY 1–695 is described accurately by the Tsallis distribution of nonextensive statistical mechanics. The Tsallis distribution also describes the *V1* observations for DOY 1–512 [which excludes the large sinusoid in $B(t)$] and the *V2* observations for DOY 1–705. The nonextensivity exponent is the same for all of these cases, $q \approx 5/3$.

The distribution of daily averages of δ measured by *V1* in the heliosheath and *V2* in the solar wind have the same SD (30° and 31°, respectively), but the averages (1° and −20°, respectively) and the shapes of the distributions are different. The differences simply reflect the uncertainties in the measurements of angles by *V1* and *V2*. The SD gives an upper limit on the size of the fluctuations in δ.

A sector pattern is evident in the *V1* data, and the percentage of negative polarity increases with time from 2005.0–2006.9. Both positive and negative polarities for λ are also observed in the *V2* data, but there is no significant change in the percentage of negative polarity, which is 40% throughout the 705 day interval. The observed polarity patterns are consistent with the position and motion of the HCS computed by Hoeksema (1991, 1995) using the "classical model" and solar magnetic field observations from the Wilcox Solar Observatory. The observations were made during the declining phase of the cycle, when the latitudinal extent of the HCS was decreasing. The maximum latitudinal extent of the HCS moved toward and possibly past *V1* at ≈N34°, resulting in an increase in the percentage of negative magnetic polarity. We expect that *V1* will observe predominantly negative polarities during 2008. The maximum extent of the HCS remained above *V2* at S26° throughout the interval, consistent with the persistence of both positive and negative polarities and the relative constancy of their relative percentage at *V2*.

N. F. Ness was partially supported by grant NNG 05-GK25G to the Catholic University of America. T. McClanahan and S. Kramer provided support in the processing of the data. Daniel Berdichevsky computed the zero-level corrections for the instrument. N. V. Pogorelov provided plots of $B(t)$ in the heliosheath predicted by his model, and discussions with him were very helpful. The magnetic field data from *ACE* were provided by the principal investigator C. Smith. We thank J. T. Hoeksema (WSO/Stanford) for providing his results on the positions of the heliospheric current sheet.

REFERENCES

Altschuler, M. D., & Newkirk, G., Jr. 1969, Sol. Phys., 9, 131
Axford, W. I. 1972, in Solar Wind, ed. C. P. Sonett, P. J. Coleman, & J. M. Wilcox (Washington: NASA), 609
Balogh, A., & Smith, E. J. 2001, Space Sci. Rev., 97, 147
Behannon, K. W., Acuña, M. H., Burlaga, L. F., Lepping, R. P., Ness, N. F., & Neubauer, F. M. 1977, Space Sci. Rev., 21, 235
Behannon, K. W., Burlaga, L. F., Hoeksema, J. T., & Klein, L. W. 1989, J. Geophys. Res., 94, 1245
Bruno, R., Burlaga, L. F., & Hundhausen, A. J. 1982, J. Geophys. Res., 87, 10339
Burlaga, L. F. 1995, Interplanetary Magnetohydrodynamics (Oxford: Oxford Univ. Press)
———. 2001, J. Geophys. Res., 106, 15917
Burlaga, L. F., Hundhausen, A. J., & Zhao, X.-P. 1981, J. Geophys. Res., 86, 8893
Burlaga, L. F., & Ness, N. F. 1993, J. Geophys. Res., 98, 17451
———. 1996, J. Geophys. Res., 101, 13473
———. 1997, J. Geophys. Res., 102, 19731
———. 1998, Space Sci. Rev., 83, 105
Burlaga, L. F., Ness, N. F., & Acuña, M. H. 2006a, Geophys. Res. Lett., 33, L21106
———. 2006b, ApJ, 642, 584
———. 2006c, J. Geophys. Res., 111, A09112
Burlaga, L. F., Ness, N. F., Acuña, M. H., Lepping, R. P., Connerney, J. E. P., Stone, E. C., & McDonald, F. B. 2005, Science, 309, 2027
Burlaga, L. F., Ness, N. F., Wang, Y.-M., & Sheeley, N. R., Jr. 2002, J. Geophys. Res. Space Physics, 107, A111410
Burlaga, L., & Viñas, A. 2005a, Physica A, 356, 375
———. 2005b, J. Geophys. Res., 110, A07110
Burlaga, L., Viñas, A., Ness, N., & Acuña, M. H. 2006d, ApJ, 644, L83
Decker, R. B., et al. 2005, Science, 309, 2020
Gurnett, D. A., & Kurth, W. S. 2005, Science, 309, 2025
Hoeksema, J. T. 1991, Adv. Space Res., 11, 15
———. 1995, Space Sci. Rev., 72, 137
Hundhausen, A. J. 1972, Coronal Expansion and Solar Wind (New York: Springer)
———. 1977, in Coronal Holes and High Speed Wind Streams, ed. J. B. Zirker (Boulder: Colo. Assoc. Univ. Press), 225
Izmodenov, V., & Alexashov, D. 2006, in AIP Conf. Proc. 858, Physics of the Inner Heliosheath, ed. J. Heerikhuisen (Berlin: Springer), 14
Izmodenov, V., Malama, Y., & Ruderman, M. S. 2005, A&A, 429, 1069
Jokipii, J. R. 2005, ApJ, 631, L163
Leroy, M. M. 1983, Phys. Fluids, 26, 2742
Liewer, P. C., Goldstein, B. E., & Omidi, N. 1993, J. Geophys. Res., 98, 15211
Liewer, P. C., Karmesin, S. R., & Brackbill, J. U. 1996, J. Geophys. Res., 101, 17119
Müller, H. R., Zank, G., Faurot-Pigeon, P., Jiwariyavej, V., Mutiso, R., & Shafi, F. 2006, in AIP Conf. Proc. 858, Physics of the Inner Heliosheath, ed. J. Heerikhuisen (Berlin: Springer), 33
Nerney, S., Suess, S. T., & Schmahl, E. J. 1991, A&A, 250, 556
———. 1993, J. Geophys. Res., 98, 15169
———. 1995, J. Geophys. Res., 100, 3463
Ness, N. F., & Burlaga, L. F. 2001, J. Geophys. Res., 106, 15803
Ness, N. F., & Wilcox, J. M. 1964, Phys. Rev. Lett., 13, 461
Opher, M., Stone, E., Liewer, P. C., & Gombosi, T. I. 2006, in AIP Conf. Proc. 858, Physics of the Inner Heliosheath, ed. J. Heerikhuisen (Berlin: Springer), 45
Opher, M., et al. 2004, ApJ, 611, 575
Parker, E. N. 1963, Interplanetary Dynamical Processes (New York: Interscience)
Pauls, H. L., Zank, G. P., & Williams, L. L. 1995, J. Geophys. Res., 100, 21595
Pogorelov, N. V. 2006, in AIP Conf. Proc. 858, Physics of the Inner Heliosheath, ed. J. Heerikhuisen (Berlin: Springer), 3
Pogorelov, N. V., Zank, G. P., & Ogino, T. 2006, ApJ, 644, 1299
Richardson, J. D., Liu, Y., & Wang, C. 2007, Adv. Space Res., submitted
Schatten, K. H., Wilcox, J. M., & Ness, N. F. 1969, Sol. Phys., 6, 443
Schulz, M. 1973, Ap&SS, 34, 371
Smith, E. J. 2001, J. Geophys. Res., 106, 15819
Smith, E. J., Balogh, A. Forsyth, R. J., & McComas, D. J. 2001, Geophys. Res. Lett., 28, 4159
Smith, E. J., Jokipii, J. R. Kota, J. Lepping, R. P., & Szabo, A. 2000, ApJ, 533, 1084
Smith, E. J., Neugebauer, M., Balogh, A., Bame, S. J., Erdös, G., Forsyth, R. J., & Goldstein, B. 1993, Geophys. Res. Lett., 20, 2327
Smith, E. J., Tsurutani, B. J., & Rosenberg, R. L. 1978, J. Geophys. Res., 83, 71
Smith, E. J., Winterhalter, D., & Slavin, J. A. 1988, in The Sixth International Solar Wind Conf., ed. V. J. Pizzo, T. E. Holzer, & D. G. Sime (NCAR Tech. Note 306; Boulder: NCAR), 581
Stone, E. C., Cummings, A. C., McDonald, F. B., Heikkila, B. C., Lal, N., & Webber, W. R. 2005, Science, 309, 2017
Tanaka, T., & Washimi, H. 1999, J. Geophys. Res., 104, 12605
Tsallis, C. 1988, J. Stat. Phys., 52, 479
Villante, E., Bruno, R., Mariani, F., Burlaga, L. F., & Ness, N. F. 1979, J. Geophys. Res., 84, 6641
Wang, Y.-M., & Sheeley, N. R. 1992, ApJ, 392, 310
Washimi, H. 1993, Adv. Space Res., 13, 227
Washimi, H., & Tanaka, T. 1996, Space. Sci. Rev., 78, 85

Washimi, H., & Tanaka, T. 1999, in Transport of Galactic and Anomalous Cosmic Rays in the Heliosphere, ed. M. S. Potgieter (Oxford: Pergamon), 551
Whang, Y. C., Burlaga, L. F., & Ness, N. F. 1995, J. Geophys. Res., 100, 17015
Whang, Y. C., Burlaga, L. F., Wang, Y. M., & Sheeley, N. R. 2004, Geophys. Res. Lett., 31, L03805
Zank, G. P. 1999, Space Sci. Rev., 89, 413
Zank, G. P., Pauls, H. L.,Williams, L. L., & Hall, D. T. 1996, J. Geophys. Res., 101, 21639